



# Bone marrow mesenchymal stem cells enrich breast cancer stem cell population via targeting metabolic pathways

Zahra Ghanbari Movahed<sup>1,2</sup> · Kamran Mansouri<sup>5</sup> · Ali Hamrahi Mohsen<sup>3</sup> · Maryam M. Matin<sup>1,4</sup>

Received: 26 October 2024 / Accepted: 13 February 2025

© The Author(s), under exclusive licence to Springer Science+Business Media, LLC, part of Springer Nature 2025

## Abstract

The role of cancer cell metabolic reprogramming in the formation and maintenance of cancer stem cells (CSCs) has been well established. This reprogramming involves alterations in the metabolic pathways of cancer cells, leading to the acquisition of stem cell-like properties such as self-renewal and differentiation. This study aimed to investigate the potential effects of bone marrow mesenchymal stem cells (BM-MSCs) on the enrichment of breast CSCs. Exosomes (Exo) and conditioned media (CM) were isolated from BM-MSCs for use in this experimental study. The impact of BM-MSCs-Exo and BM-MSCs-CM on the expression of stemness genes *NANOG* and *OCT-4*, as well as CD24 and CD44 markers, was assessed in MCF-7 and MDA-MB-231 cell cultures to identify CSCs. Furthermore, the effects of BM-MSCs-Exo and BM-MSCs-CM on cancer cell metabolism were evaluated by examining changes in glycolysis, the pentose phosphate pathway (PPP), and amino acid profiles. Additionally, the influence of BM-MSCs-Exo and BM-MSCs-CM on tumor growth in vivo was also investigated. The analysis of stemness marker expression in cells treated with BM-MSCs-Exo and BM-MSCs-CM revealed an increase in stemness characteristics compared to the control group. Furthermore, the examination of changes in cell metabolism following these treatments showed alterations in glycolysis, PPP, and amino acid metabolism pathways. Additionally, it was demonstrated that BM-MSCs-Exo and BM-MSCs-CM can promote tumor growth in mice following transplantation of 4T1 cells. These findings suggest that BM-MSCs-Exo and BM-MSCs-CM can enrich the population of CSCs in MCF-7 and MDA-MB-231 cells by targeting metabolic pathways, however, further studies are required to elicit the exact mechanisms of these phenomena.

**Keywords** Cancer stem cells · Conditioned media · Metabolism · BM-MSCs · Breast cancer cells · Exosomes

## Introduction

Mesenchymal stem cells (MSCs) were initially identified within the bone marrow stroma during the 1960s [1]. MSCs are multipotent progenitor cells that contribute to the normal homeostasis and reconstruction of tissues [2]. Various models have been employed to validate the safety and efficacy of

MSCs derived from the bone marrow, owing to their potential for clinical applications [3, 4]. Earlier investigations demonstrated that the use of bone marrow-derived MSCs does not confer a distinct risk of tumorigenesis when used for treatment of various diseases [5, 6]. Nevertheless, some studies have suggested that MSCs derived from the bone marrow promote the development, proliferation, migration,

✉ Kamran Mansouri  
kmansouri@kums.ac.ir

✉ Maryam M. Matin  
Matin@um.ac.ir

Zahra Ghanbari Movahed  
Zahra.gh.movahed@gmail.com

Ali Hamrahi Mohsen  
hamrahi.ali.1992@gmail.com

<sup>1</sup> Department of Biology, Faculty of Science, Ferdowsi University of Mashhad, Mashhad, Iran

<sup>2</sup> Medical Biology Research Center, Kermanshah University of Medical Sciences, Bākhtarān, Iran

<sup>3</sup> Institute of Biochemistry and Biophysics, Faculty of Science, University of Tehran, Tehran, Iran

<sup>4</sup> Novel Diagnostics and Therapeutics Research Group, Institute of Biotechnology, Ferdowsi University of Mashhad, Mashhad, Iran

<sup>5</sup> Medical Biology Research Center, Health Technology Institute, School of Medicine, Kermanshah University of Medical Sciences, P.O. Box 67145-1673, Bākhtarān, Iran

and stemness properties of cancer cells [7–9]. In one study it was shown that Mesenchymal stem cells confer chemoresistance in breast cancer via a CD9-dependent mechanism [10]. Moreover, BM-MSCs were able to stimulate cancer cell growth and angiogenesis. In breast tumors, for example, BM-MSCs raised the amounts of pro-angiogenic factors, such as MIP-2, VEGF, TGF- $\beta$  and IL-6. These factors induced tumor cells proliferation and angiogenesis, thereby increasing the pace of solid tumor development in vitro and in vivo [11]. Paracrine signaling is one of the potential mechanisms through which MSCs influence tumor initiation and progression. In several investigations, it has been confirmed that MSCs facilitate the migration and advancement of different types of cancers via paracrine mechanisms, such as exosomes and some secreted factors present in the culture medium [9, 12]. In one study, it was shown that both co-culturing with mice BM-MSCs (mBM-MSCs) and treatment with mBM-MSC-conditioned medium enhanced the growth of 4T1 cells [11]. Also, BM-MSC-derived exosomes induced by breast cancer cells promoted breast cancer dormancy by transferring miR-222/223 in vitro and in vivo, and this dormancy was linked to carboplatin resistance [13].

Exosomes, small vesicles measuring 30–200 nm, are secreted into the extracellular space by a variety of cell types [14, 15]. These exosomes are filled with proteins, lipids, and nucleic acids, including genomic DNA, microRNAs (miRNAs), mRNAs, long non-coding RNAs (lncRNAs), mitochondrial DNA (mtDNA), and cDNA [16, 17]. The role of exosomes in facilitating cell-to-cell communication is of utmost importance. They can be internalized by recipient cells or transported to distant locations through biological fluids, potentially resulting in phenotypic changes in the recipient cells [18, 19]. Exosomes also have the ability to transfer functional molecules to tumor cells, thereby promoting angiogenesis, tumor progression, drug resistance, metastasis, and immunosuppression through reprogramming of cancer cell metabolism [20]. Metabolic reprogramming is a characteristic feature of tumor progression, as it supports cell viability, proliferation, and tumorigenesis [21]. Similarly, metabolic reprogramming plays a crucial role in the conversion of cancer cells to cancer stem cells (CSCs) [22].

## Materials and methods

### Cell culture and culture conditions

MCF-7, MDA-MB-231, BM-MSCs, and fibroblast cells were procured from Royan ATMP-TDC (Tehran, Iran). All cells were cultivated in complete Dulbecco's modified Eagle's medium/nutrient mixture F12 (DMEM/F12) medium supplemented with 10% fetal bovine serum (FBS), penicillin (100 U/mL), and streptomycin (100 mg/mL) (P/S)

at the temperature of 37 °C in a controlled environment with 5% CO<sub>2</sub>.

### Cancer cell spheroid culture

The process of cultivating cancer cell spheroids involved the combination of 1% agarose powder from Sigma with DMEM/F12, which was subsequently subjected to autoclave sterilization. Upon the solution liquid state, 1.5 mL of the solution was carefully added to 6-well culture Petri dishes (SARSTEDT, Germany). Following solidification, cell suspensions containing MCF-7 and MDA-MB-231 cells at a concentration of  $5 \times 10^5$  cells/mL, supplemented with 5% FBS and 1% P/S, were meticulously introduced into the 6-well culture Petri dishes. The culture dishes were then placed in a 37 °C incubator with 5% CO<sub>2</sub>. After 48 h, nearly all cancer cells had formed spheroids, which were subsequently collected for further experimentation or delicately transferred to new non-adhesive plastic Petri dishes (SARSTEDT, Germany) for the purpose of capturing images. The aim of the present study was to assess the impact of BM-MSCs on the enrichment of the CSC population in breast cancer cells. Moreover, an investigation was conducted to examine the influence of these treatments on the induction of CSCs through alteration of the metabolism.

### Drug sensitivity assay

The evaluation of chemotherapeutic drug sensitivity in spheroids and monolayer cells was conducted using the MTT (3-(4,5-dimethyl-2-thiazolyl)-2,5-diphenyl-2H-tetrazolium bromide) (Merck, Germany) assay. Both the monolayer and spheroid cells were cultivated in 96-well microplates with a comparable cell culture medium. However, for the spheroids, the individual cells were placed in a 96-well plate coated with agarose. The cells were then counted and seeded into 96-well plates, with a density of  $5 \times 10^3$  cells per well. Subsequently, the cultures were treated with varying concentrations (ranging from 0 to 100  $\mu$ g/mL) of doxorubicin (EBEWE Pharma, Austria). As a control, the diluent alone, DMEM, was utilized. The standard MTT assay was performed for monolayer cells [23], while a slightly adapted version was employed for spheroids [24]. The determination of cytotoxicity was conducted through analysis of the average absorbance of the treated cells in relation to the controls, which were regarded as exhibiting 100% viability. This analysis was then converted into a percentage representing cell viability. The visualization of the treated spheroids was accomplished through an inverted microscope, with observations being made at various concentrations of the administered drug 24 h post-treatment. As a reference, untreated cells were cultured in parallel to the experiments, with all procedures being conducted in triplicate.

## Quantitative RT-PCR

The process of quantitative RT-PCR involved the extraction of total RNA from the MCF-7 and MDA-MB-231 cell lines using the RNXPlus kit manufactured by Sinnaclon (Iran). DNase I (STEMCELL Technologies, Canada) was used to reduce the probability of primers binding to genomic DNA, and followed by cDNA synthesis. ExcelRT™ *Reverse Transcription Kit* (SMOBIO, Taiwan) was used for this purpose. Subsequently, the quantitative RT-PCR was conducted using the SYBR Green RT-PCR Master Mix (Yekta Tajhizazma, Iran) on the Corbett Rotor-Gene 6000 thermal cycler (Corbett Research, Australia). To perform the quantitative RT-PCR, specific primer sequences were designed for *NANOG* and *OCT-4* with the primer sequences obtained from NCBI. The mRNA expression levels were normalized to the levels of endogenous  $\beta$ -*ACTIN* mRNA. The following primers were used in this study:

*NANOG*: forward 5'-TGAGATGCCTCACACGGAGAC-3' and reverse 5'-GGTTGTTTGCCTTTGGGACTG-3'; *OCT-4*: forward 5'-GGTGCCTGCCCTTCTAGGAATG-3' and reverse 5'-TGCCCCACCCCTTTGTGTTC-3'; *Beta-ACTIN*: forward 5'-ACCTTCTACAATGAGCTGCG-3' and reverse 5'-CCTGGATAGCAACGTACATGG-3'.

## Flow cytometry

In order to compare the characteristics of adherent cells with spheroid cells, the ratio of CD44<sup>+</sup>/CD24<sup>-</sup> surface markers was assessed using flow cytometry. Both the adherent and spheroid populations were detached into single cells using 0.05% trypsin/0.02% ethylenediaminetetraacetic acid (EDTA), followed by centrifugation and suspension in 2% bovine serum albumin (BSA) in PBS. Fluorochrome-conjugated monoclonal antibodies, namely FITC anti-human CD44 and PE anti-human CD24 (BD Pharmingen, England), were added to the cell suspension and incubated in the dark at 4 °C for 30 min. The cells were then centrifuged and washed three times before examination. Based on their surface markers, cells were sorted into subpopulations of CD44<sup>+</sup>/CD24<sup>-</sup>. Furthermore, to evaluate the impact of BM-MSCs-Exo and BM-MSCs-CM on the CD44<sup>+</sup>/CD24<sup>-</sup> subpopulations, 2 × 10<sup>5</sup> cells/well were seeded into 6-well plates for 1 day. Subsequently, the cells were treated with 20 µg/mL BM-MSCs-Exo and 0.5 mg/mL BM-MSCs-CM for 1 day. The distribution was finally evaluated using an Attune NxT flow cytometer (Thermo Fisher Scientific, USA), and the data were analyzed using FlowJo™ 10 software.

## Preparing the conditioned medium (CM)

Both cell lines were suspended in DMEM-F12 supplemented with 5% FBS and 1% P/S. For monolayer culture, 3 × 10<sup>5</sup>

cells/well (500 µL of the cell suspensions) were seeded in 24-well plates and incubated for 2 days. The same procedure was employed for spheroids, however, cells were seeded in 24-well plates coated with agarose. After 2 days, the monolayer and spheroid cells were washed with PBS and 500 µL of serum-free medium was added to the plates. After 1 day, 200 µL of the CM was collected from both cultures, followed by centrifugation at 200×g for 10 min, concentrated 25 times using 10-kDa MW cutoff ultrafiltration membranes and sterilized by filtration through a 220-nm filter and then stored at -80 °C. The protein concentration was measured using the Bradford method. The control group consisted of the serum-free DMEM-F12, which was incubated at 37 °C for 1 day and subsequently stored at -80 °C.

## In vitro cytotoxicity assay

MTT assay was performed to test the in vitro cytotoxicity of BM-MSCs-CM against 4T1, MCF-7, and MDA-MB-231 cell lines, as well as normal fibroblast cells. Cells were incubated overnight at 37 °C with 5% CO<sub>2</sub> in a 96-well plate containing 10<sup>4</sup> cells/well. The following day BM-MSCs-CM was added in varying concentrations to the wells. After 24 and 48 h of incubation, MTT assay was performed. The data from the viability assays was reported as a percentage of the control counts. All assays were performed in triplicate and the results were obtained from three independent experiments.

## Isolation of exosomes from BM-MSCs

BM-MSCs were cultured until they reached 80% confluence in a complete medium. Subsequently, the culture medium was replaced with a serum-free medium. After 2 days, the exosomes from the culture medium of BM-MSCs were isolated using the polyethylene glycol (PEG) precipitation method. To prepare a 40% PEG solution, 40 g of PEG 6000 (Merck, Germany) was added to 100 mL of PBS. A mixture of 10 mL prefiltered medium and 2.5 mL of the 40% PEG solution was prepared to obtain an 8% PEG-medium solution. This solution was then incubated overnight at 4 °C and subsequently centrifuged at 4 °C for 90 min at 4000×g. The supernatant was discarded, and the exosome pellet was suspended in 250 µL of particle-free PBS and stored at -80 °C. The concentration of exosomes was assessed using a NanoDrop.

## DLS assay

The extracted exosomes were diluted to a concentration of 0.1 µg/µL using PBS. Once the laser and temperature of the device reached equilibrium, the exosome-containing cuvette

was inserted into the DLS device (Dynapro Nanostar, WYATT Technology) to initiate the measurement.

### Transmission electron microscopy (TEM)

Transmission electron microscopy (TEM) was utilized to validate the presence and morphology of the exosomes. Briefly, 10  $\mu\text{g}$  of exosomes were placed on a copper grid and subjected to negative staining with 2% uranyl acetate for 2 min at room temperature. The grids were then rinsed with deionized water and left to dry overnight. The visualization of the samples was performed using a Hitachi S-3000 N electron microscope.

### Western blot assay

Western blotting was employed to detect exosome marker proteins, including CD9, CD63, and CD81. Total proteins were extracted and quantified using a Bicinchoninic acid (BCA) kit (Parstous, Iran) and a lysis buffer (Proteintech, Germany). The proteins were separated using sodium dodecyl sulfate–polyacrylamide gel electrophoresis (SDS-PAGE) and transferred to a nitrocellulose membrane (Abcam, UK). The membranes were then blocked with 5% BSA (Merck, Germany) at 37 °C for 1 h and incubated overnight at 4 °C with primary antibodies Anti-CD9 (NBP1-00748, Novus, USA), Anti-CD63 antibody (ab59479, Abcam, UK) and Anti-CD81 (sc-166029, Santa Cruz Biotechnology, USA) at a dilution of 1/2000. Subsequently, the membranes were incubated with the secondary antibody Goat Anti-Human IgG H&L (ab97161, Abcam, UK) at a dilution of 1/2000. The bands were visualized by exposing the membranes to X-ray films (SABZ Biomedicals, Iran).

### Intracellular ROS assay

The measurement of ROS was conducted using 2',7'-dichlorofluorescein diacetate (DCFDA). DCFDA is a fluorogenic dye that is deacetylated by esterases, resulting in the formation of a non-fluorescent compound. The oxidation of this compound by ROS leads to the generation of a highly fluorescent element known as 2',7'-dichlorofluorescein (DCF), which emits green fluorescence. The level of ROS was determined by measuring the intensity of the emitted fluorescence [25]. The cells were rinsed with PBS (pH 7.4) 1 day after treatment with 20  $\mu\text{g}/\text{mL}$  BM-MSCs-Exo and 0.5  $\text{mg}/\text{mL}$  BM-MSCs-CM. Subsequently, the cells were incubated at 37 °C for 30 min with 20  $\mu\text{L}$  of DCFDA. Cells were then lysed with Triton X-100, and the fluorescence was assessed using an Attune NxT flow cytometer (Thermo Fisher Scientific, USA) with an excitation wavelength of 488 nm and an emission wavelength of 528 nm. The data were analyzed using the FlowJo™ 10 software.

### Lactate assay

For the lactate concentration assay, an enzymatic color test was performed using the lactate colorimetric kit according to the manufacturer's instructions (BIOREXFARS, Iran). After one day of treatment with 20  $\mu\text{g}/\text{mL}$  BM-MSCs-Exo and 0.5  $\text{mg}/\text{mL}$  BM-MSCs-CM, the cell supernatants from each treated well were collected and used for the respective assays. The concentration of lactate in the supernatants was evaluated spectrophotometrically at 545 nm.

### G6PD enzyme activity assay

The activity of the G6PD enzyme was determined by measuring the rate of NADPH production in cell supernatants using a specific kit (Baharafshan, Iran) as per the provided instructions. G6PD is a cytosolic enzyme that catalyzes the conversion of D-glucose 6-phosphate + NADP<sup>+</sup> to 6-phospho-D-glucono-1,5-lactone + NADPH + H<sup>+</sup> in the pentose phosphate pathway. Therefore, the activity of G6PD enzyme was evaluated by measuring the enhanced absorption at 340 nm, which is indicative of the decreased conversion of NADP<sup>+</sup> to NADPH by this enzyme.

### Amino acid profile assay

The amino acid profile assay involved the addition of 0.1 mL trichloro acetic acid (TCA) (Merck, Germany) per 1 mL of supernatant to precipitate proteins. Subsequently, centrifugation was conducted at 600 $\times g$  for 10 min. The supernatants were collected and placed on ice for amino acid analysis via high-performance liquid chromatography (HPLC) using the YL9100 system (Young Lin, Korea). Chromatographic separation of amino acids was accomplished using a C18 column (25 cm long  $\times$  4.0 mm i.d., 5  $\mu\text{m}$ , GL Sciences, Japan).

### Animal study

For the animal study, female BALB/c mice (20–25 g) were obtained from Pasture Institute (Iran) and used in the experiments. The animals were housed in temperature-controlled rooms (22–25 °C) with a 12:12 h light–dark cycle and provided with standard food and water.

Six-week-old female BALB/c mice were injected with murine breast tumor 4T1 cells ( $1 \times 10^5$  cells/mouse). Two weeks later, mice were treated every 2 days with PBS, exosomes (0.0005  $\text{mg}/\text{kg}$ ) and CM (0.025  $\text{mg}/\text{kg}$ ) by intravenous tail injection, for 1 week. After that, the animals were sacrificed, and the tumors were measured.

**Fig. 1** Characterization of spheroids produced from MCF-7 and MDA-MB-231 breast cancer cell lines. The morphology of MCF-7 and MDA-MB-231 spheroids is depicted in panel **A**. Panel **B** illustrates the integrity and viability of spheroids after treatment with the chemotherapeutic drug doxorubicin at a concentration of 30 µg/mL. The transcript levels of *NANOG* and *OCT-4* in MCF-7 and MDA-MB-231 spheroids, compared to adherent cells, were quantified via real-time PCR, as shown in panel **C**. The flow cytometry analysis of CD44<sup>+</sup>/CD24<sup>-</sup> status in MCF-7 and MDA-MB-231 spheroids is presented in panel **D**. The results are presented as the mean ± SD of three independent experiments (\*\**p* < 0.001)

**Statistical analysis**

Statistical analysis was conducted using GraphPad Prism 8.0.2 software. One-way ANOVA followed by Tukey’s multiple comparisons test was performed to compare the groups.

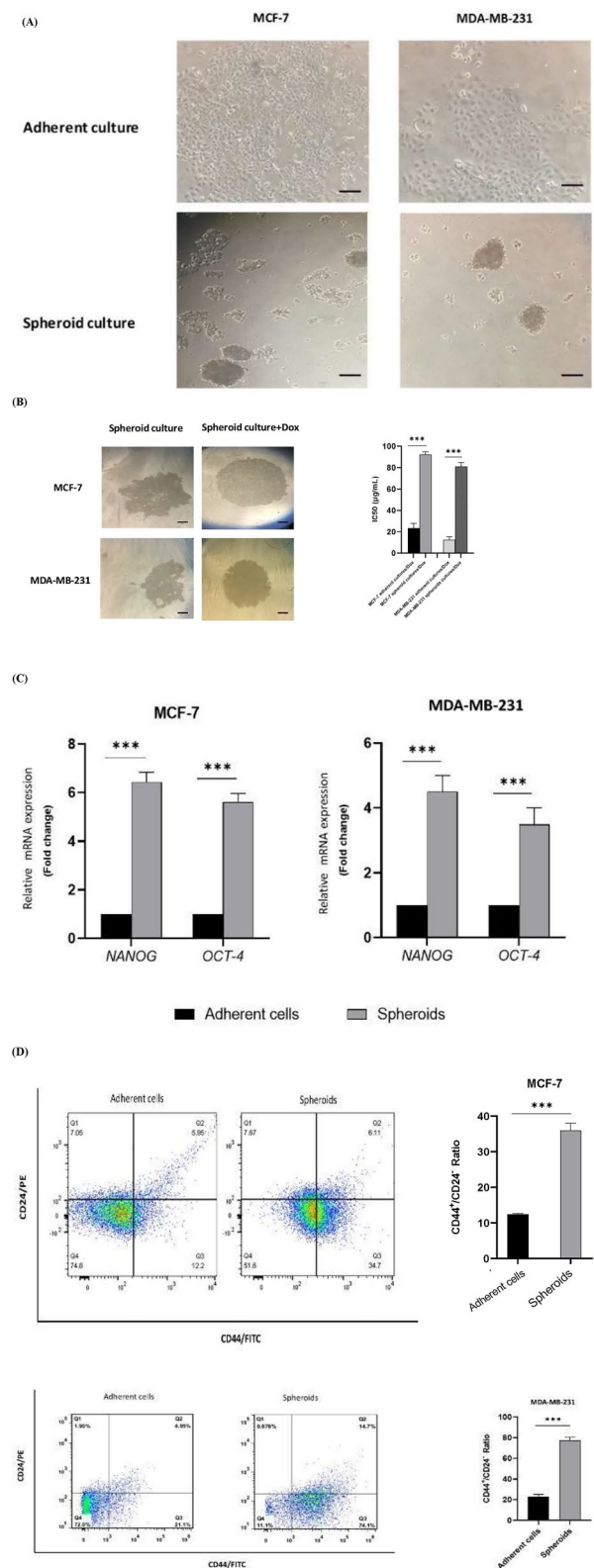
**Results**

**Certification of spheroid formation**

Spheroids were obtained from MCF-7 and MDA-MB-231 cells. These spheroids were characterized by analyzing their resistance to doxorubicin, examining the expression of two stem cell markers, namely *NANOG* and *OCT-4*, and studying the cell surface markers CD44 and CD24, which are common in breast CSCs. The findings revealed that spheroid cultures exhibited greater resistance to doxorubicin treatment compared to adherent cultures in both cell lines. Furthermore, the expression of *NANOG* and *OCT-4* was significantly higher in spheroids than in adherent cultures. Additionally, flow cytometry analysis demonstrated a considerable increase in the proportion of CD44<sup>+</sup>/CD24<sup>-</sup> cells in spheroids compared to adherent cultures in both cell lines. Specifically, this proportion increased from 14.1 to 50% for MCF-7 and from 21.1 to 74.1% for MDA-MB-231 cells (Fig. 1). These results suggest that spheroids are enriched with cancer stem-like cells, making them suitable for further experimentation.

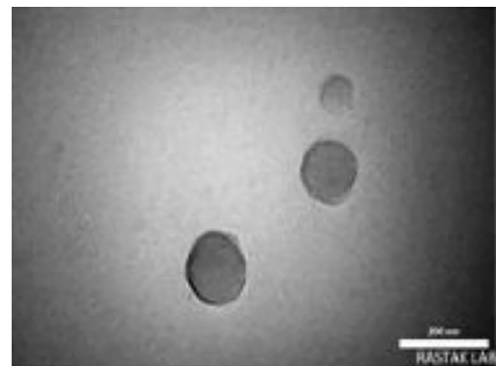
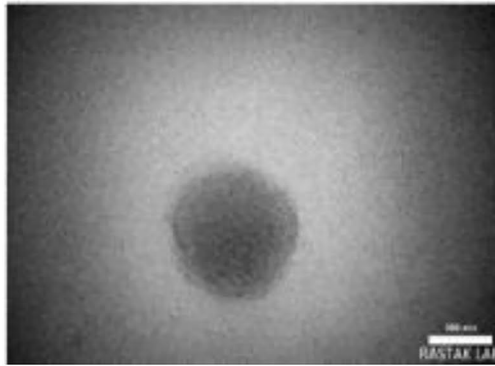
**Characterization of BM-MSCs-Exo**

The morphology of exosomes was assessed using TEM. As shown in Fig. 2A, BM-MSCs-Exo are bilayered membrane structures ranging in diameter from 30 to 200 nm. The size distribution of exosomes was determined using DLS, which revealed a range of sizes between 40 and 280 nm in diameter (Fig. 2B). Western blot analysis confirmed the presence of

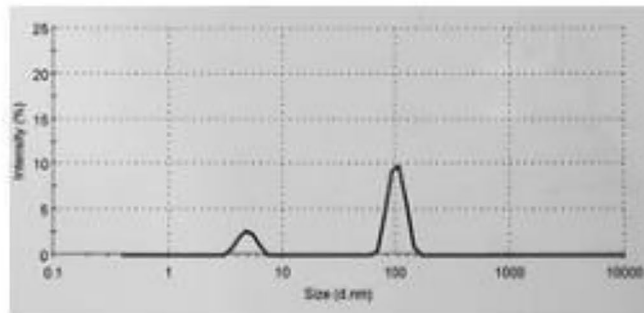


exosome markers CD9, CD63, and CD81 on the surface of BM-MSCs-Exo (Fig. 2C).

(A)



(B)



(C)

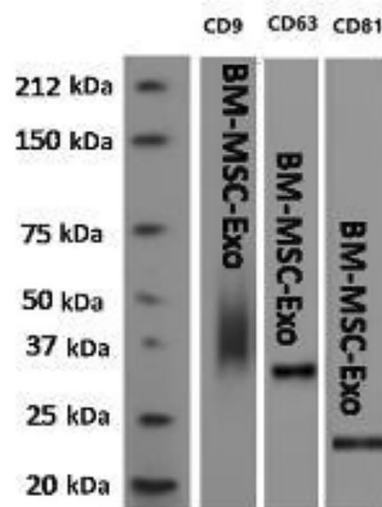


**Fig. 2** Characterization of exosomes. TEM was used to observe the heterogeneous size mixture of discrete vesicles, ranging from approximately 30 to 200 nm, as displayed in panel A (scale bar: 200 and 500  $\mu\text{m}$ ). DLS analysis confirmed the presence of round particles

with a size distribution within the defined range for exosomes (30–200 nm), as shown in panel B. Western blot results in panel C demonstrate the presence of positive exosome markers CD9, CD63, and CD81

### The impact of BM-MSCs-CM on cell viability

To assess the cytotoxicity of BM-MSCs-CM (0.5 mg/mL), the MTT assay was performed on 4T1, MCF-7, and

MDA-MB-231 cell lines, as well as normal fibroblast cells, at two selected time points (Fig. 3). The results indicated that cell viability was not significantly reduced in cells treated with BM-MSCs-CM after 24 and 48 h.

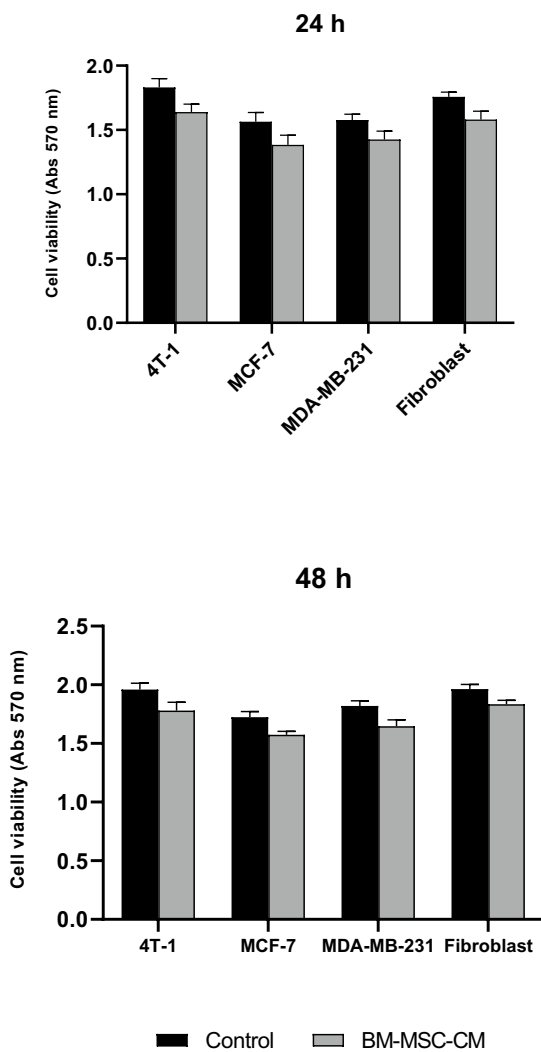


**Fig. 3** Evaluating the cytotoxicity of BM-MSCs-CM on different cell lines. Cell viability was assessed at different time points after treatment of various cell types with BM-MSCs-CM. The results are presented as the mean  $\pm$  SD of three independent experiments

### The effect of BM-MSCs-Exo and BM-MSCs-CM on spheroid morphology

The morphology of spheroids was examined after 24 h of culture, and microscopy images revealed distinct morphological differences between spheroids cultured in medium with and without BM-MSCs-Exo and BM-MSCs-CM. Specifically, MCF-7 and MDA-MB-231 spheroids treated with BM-MSCs-Exo and BM-MSCs-CM appeared more compact and smaller compared to untreated spheroids (Fig. 4).

### BM-MSCs-Exo and BM-MSCs-CM induced the expression of CSC markers

Following a 24-h treatment with BM-MSCs-Exo and BM-MSCs-CM, the mRNA expression of CSC markers *NANOG* and *OCT-4* was quantified using qRT-PCR. The results demonstrated an up-regulation of these genes after treatment with BM-MSCs-Exo and BM-MSCs-CM. The impact of BM-MSCs-Exo and BM-MSCs-CM treatment on the expression of cell surface markers CD44 and CD24 was also evaluated in both MCF-7 and MDA-MB-231 cells using flow cytometry. The results demonstrated that both BM-MSCs-Exo and BM-MSCs-CM significantly increased the population of CD44<sup>+</sup>/CD24<sup>-</sup> cells compared to untreated MCF-7 and MDA-MB-231 cells (Fig. 5).

### The impact of BM-MSCs-Exo and BM-MSCs-CM on lactate production and G6PD activity

After a 24-h exposure to BM-MSCs-CM, there was a notable increase in the quantity of lactate in the MCF-7 cell line. Conversely, treatment with BM-MSCs-Exo resulted in a significant reduction in lactate level in the MCF-7 cell line after 24 h. However, in the case of MDA-MB-231, there was no significant alteration observed in the pattern of lactate production following treatment with BM-MSCs-Exo and BM-MSCs-CM (Fig. 6).

According to the findings, there was a significant difference in G6PD activity between the treatment group and the control group in both the MCF-7 and MDA-MB-231 cell lines. Specifically, the activity of G6PD was significantly increased by the administration of BM-MSCs-Exo (20  $\mu$ g/mL) and BM-MSCs-CM (0.5 mg/mL) in both MCF-7 and MDA-MB-231 cell lines (Fig. 6).

### The effect of BM-MSCs-Exo and BM-MSCs-CM on ROS production

The production of ROS by MCF-7 and MDA-MB-231 cells after treatment with BM-MSCs-Exo and BM-MSCs-CM was assessed using DCFDA. The amount of ROS generated by MCF-7 and MDA-MB-231 cells showed no significant increase when treated with BM-MSCs-CM compared to the control group. However, treatment with BM-MSCs-Exo resulted in a significant decrease in ROS levels in MCF-7 cells compared to the control group. Furthermore, in MDA-MB-231 cells, there was no significant changes in ROS production following treatment with BM-MSCs-Exo (Fig. 7).

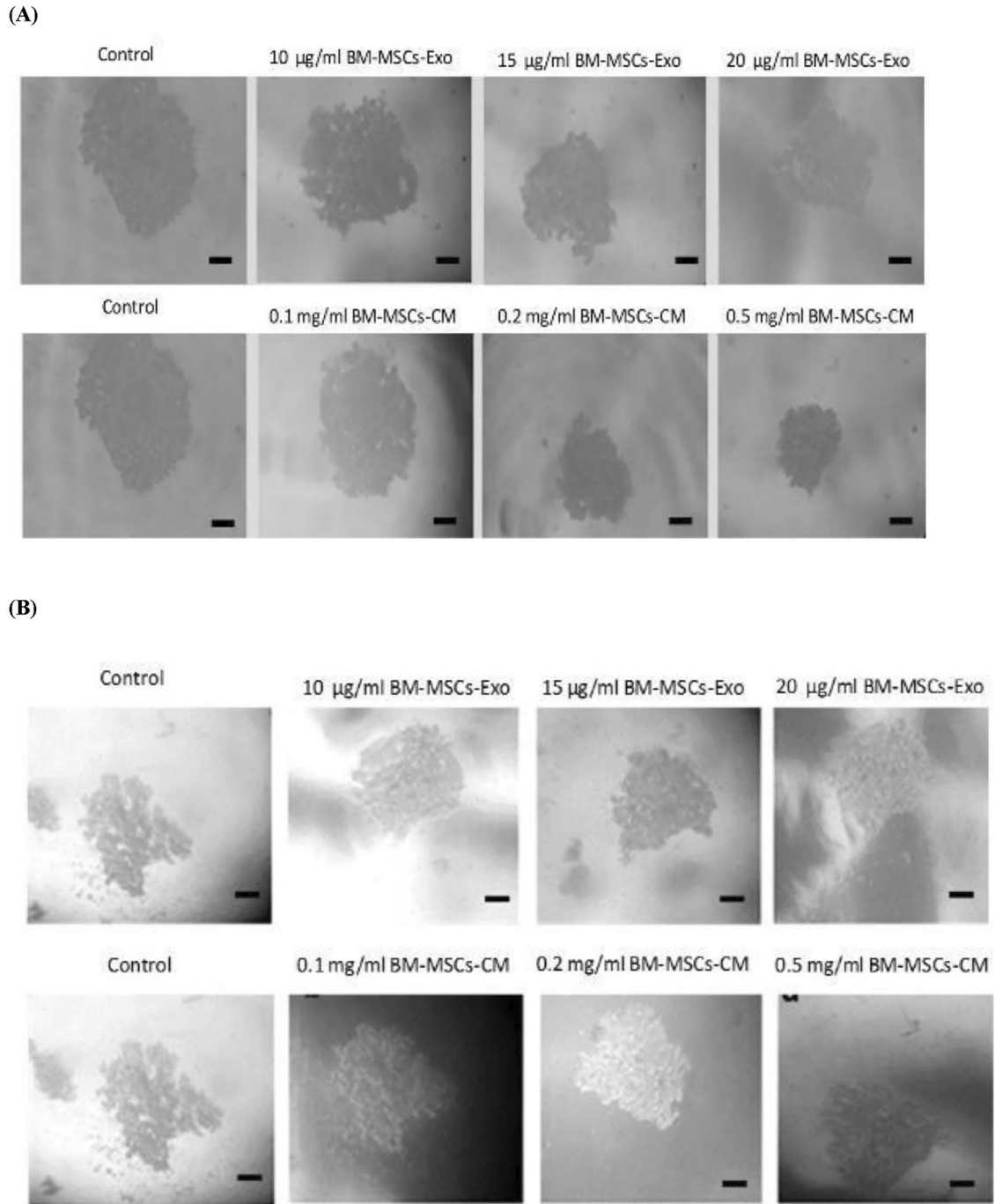


**Fig. 4** The effect of various treatments on the morphology of spheroids. Images of **A** MCF-7 and **B** MDA-MB-231 spheroids formed after 24 h of culture in various concentrations of BM-MSCs-Exo and

BM-MSCs-CM are provided. The treated spheroids exhibit a compact aggregate morphology compared to the non-treated spheroids. All images were captured at a magnification of  $\times 25$  (scale bar: 200 µm)

### BM-MSCs-Exo and BM-MSCs-CM modulated amino acid metabolism

The level of all amino acids was found to be altered when the cells were cultured with BM-MSCs-Exo and BM-MSCs-CM. Overall, treatment with BM-MSCs-Exo

and BM-MSCs-CM led to a reduction in all amino acids, except for alanine, histidine, and arginine, compared to the control group in the MCF-7 cell line. There was a significant decrease in the levels of five amino acids, including glutamine, glycine, threonine, serine, and lysine, in the groups treated with BM-MSCs-Exo and

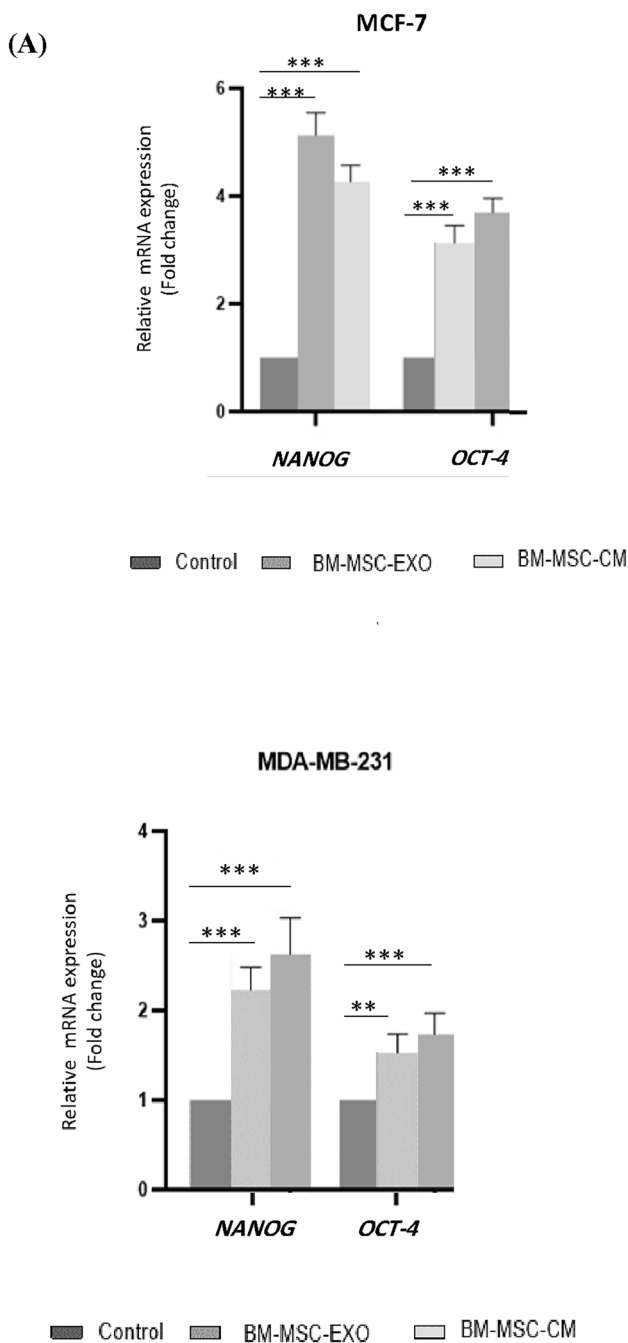


**Fig. 5** The effect of BM-MSCs-Exo and BM-MSCs-CM on CSC Markers in breast tumor cells. The impact of BM-MSCs-Exo and BM-MSCs-CM on the expression of **A** cancer stem cell markers *NANOG* and *OCT-4* and **B** Cell surface markers  $CD44^+/CD24^-$  in breast cancer cell lines. Student *t*-test was used for statistical analysis. The results are presented as the mean  $\pm$  SD of three independent experiments. The significance levels are denoted as  $*p < 0.05$ ,  $**p < 0.01$ , and  $***p < 0.001$  compared to the control

BM-MSCs-CM compared to the control group in the MCF-7 cell line. Additionally, alanine exhibited a significant increase in the BM-MSCs-Exo and BM-MSCs-CM

treated groups compared to the control group in MCF-7 cells (Fig. 8).

In the case of MDA-MB-231 cells, treatment with BM-MSCs-Exo led to a decrease in all amino acids. Only glutamine showed a significant decrease in the BM-MSCs-Exo treated group compared to the control in the MDA-MB-231 cell line. Treatment with BM-MSCs-CM resulted in a decrease in all amino acids, except for glutamic acid, lysine, histidine, and arginine, compared to the control group. Notably, histidine showed a significant increase in the BM-MSCs-CM treated group compared to the control in the MDA-MB-231 cell line. Moreover, threonine and glutamine exhibited a significant reduction in the BM-MSCs-CM treated group compared to the control (Fig. 8).

### BM-MSCs-Exo and BM-MSCs-CM promoted tumor growth in vivo

To further prove the effects of BM-MSCs-Exo and BM-MSCs-CM on tumor formation of 4T1 cells in vivo, 4T1 cells were injected subcutaneously into mice to establish a breast cancer tumor model, while BM-MSCs-Exo and BM-MSCs-CM were injected through the tail vein. Then, the formation of tumor was observed and recorded. The examination of tumor growth in vivo revealed a significant increase in tumor size and volume in the treated group compared to the control group, indicating that BM-MSCs-Exo and BM-MSCs-CM facilitated tumor growth in vivo (Fig. 9).

### Discussion

MSCs are multipotent cells that possess a significant capacity for self-renewal and differentiation, rendering them a promising population for regenerative medicine [26]. Although BM is usually considered as the primary source of MSCs, the frequency of these stem cells in this tissue is minimal [27]. Within the BM, MSCs play a vital role in supporting hematopoiesis and regulating immune activities [28]. Some studies have indicated that the interaction between MSCs and tumor cells can contribute to tumor growth, drug resistance, and metastasis. Furthermore, this interaction within the tumor microenvironment can induce a CSC phenotype in tumor cells. Various mechanisms, such as exosomes, cell-cell interactions, and paracrine secretion of molecules like cytokines, growth factors, and inflammatory mediators, are involved in the crosstalk between MSCs and tumor cells [31]. The objective of this study was to investigate the potential involvement of BM-MSCs in enrichment of CSCs in breast cancer cells.

Different mechanisms have been implicated in the induction of a stem cell phenotype in cancer cells and the restoration of CSCs, including direct transformation of MSCs into

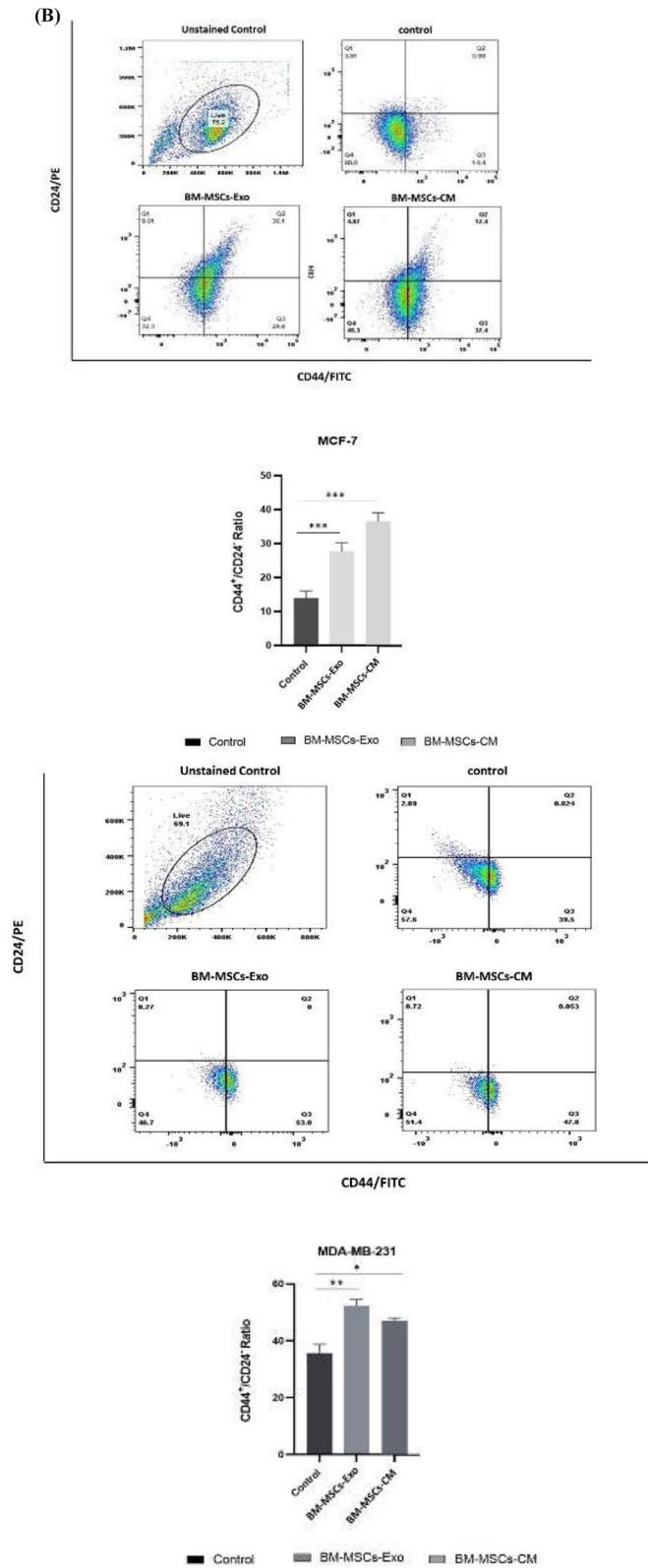
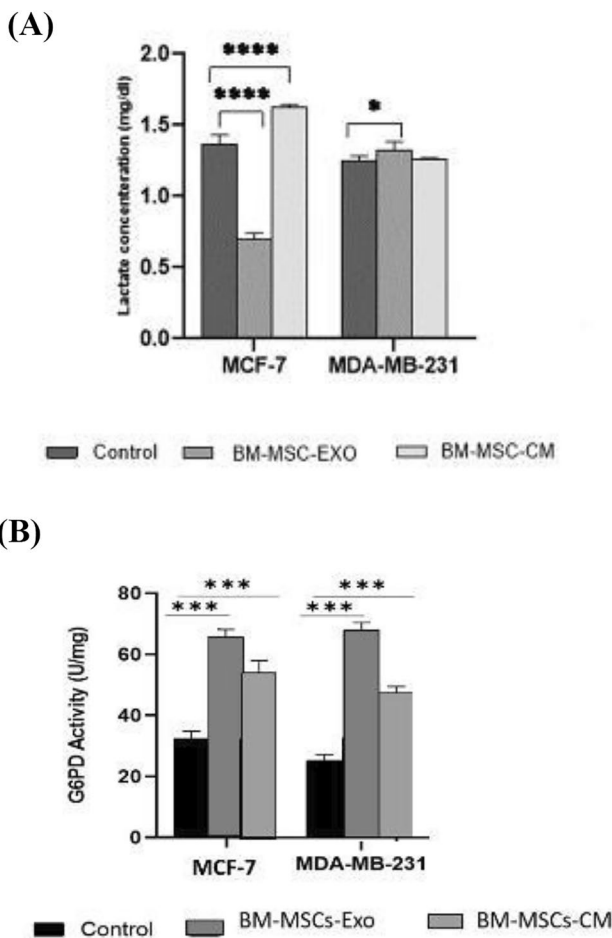


Fig. 5 (continued)



**Fig. 6** The effect of BM-MSCs-Exo and BM-MSCs-CM on glucose metabolism in breast tumor cells. Influence of BM-MSCs-Exo and BM-MSCs-CM on **A** lactate production and **B** G6PD activity in MCF-7 and MDA-MB-231 breast cancer cell lines. The lactate production and G6PD activity after 24 h of treatment with BM-MSCs-Exo and BM-MSCs-CM is compared to the controls. The results are presented as the mean ± SD of three independent experiments (\**p* < 0.05 and \*\*\**p* < 0.001)

CSCs, cell fusion, and crosstalk between MSCs and CSCs/tumor cells mediated by secretory factors and exosomes [29]. Exosomes play a crucial role in intercellular communication, as they can be taken up by neighboring cells or transported to distant sites through biological fluids, leading to phenotypic changes in recipient cells [30, 31].

In this study, we examined the crosstalk between BM-MSCs and tumor cells, focusing specifically on BM-MSCs-derived exosomes and conditioned medium. To determine the impact of BM-MSCs-Exo and BM-MSCs-CM on CSC enrichment in breast tumors, we assessed the expression of cell surface markers in MCF-7 and MDA-MB-231 cell lines, in comparison to untreated cells. Additionally, we analyzed the expression of stemness genes *NANOG* and *OCT-4*, which showed a significant increase after treatment

with BM-MSCs-Exo and BM-MSCs-CM compared to the untreated control cells. These findings provide substantial evidence for the role of these two treatments in enriching CSCs in MCF-7 and MDA-MB-231 breast cancer cells.

Previous studies have suggested that MSCs can alter tumor metabolism [32]. Therefore, in this study, we investigated the impact of BM-MSCs on the metabolic pathways of tumor cells during the enrichment of CSCs. Specifically, we examined the glycolysis, pentose phosphate, and amino acid metabolism pathways.

The assessment of lactate production was conducted to evaluate the glycolytic status of the treatment groups. BM-MSCs-Exo treatment reduced lactate production in the MCF-7 cell line by inhibiting the glycolysis pathway. It was observed that lactate production was higher in MCF-7 cells under BM-MSCs-CM treatment compared to the control group. This indicates a more active glycolysis pathway in the treatment group. The increased lactate production and glycolytic flux, even in the presence of sufficient oxygen, suggests a shift in the metabolism of breast CSCs from oxidative phosphorylation to aerobic glycolysis. Experimental evidence has shown an elevated HIF-1α in breast CSC spheres, even when oxygen is present. This, in turn, leads to higher expression of proteins involved in metabolism, glucose transport, and lactate production [33].

Furthermore, treatment with BM-MSCs-Exo and BM-MSCs-CM did not significantly alter lactate production in MDA-MB-231 cells. Studies have indicated that the metabolism of MDA-MB-231 cells is more reliant on glycolysis, while the metabolism of MCF-7 cells depends on the TCA cycle [33]. Therefore, the lack of a significant alteration in lactate production in MDA-MB-231 cells could be due to the metabolic dependence of these cells on glycolysis.

Studies have shown that tumor cells, when exposed to ROS, first activate the glycolysis pathway [22]. Our results indicated that the amount of ROS produced by MCF-7 cells was insignificantly increased in BM-MSCs-CM compared to the control group. Consequently, the increase in lactate production after treatment with BM-MSCs-CM could be attributed to the enhancement of ROS in MCF-7 cells. Studies have shown that an increase in ROS in cells increases the expression of stemness genes such as *oct4*, *sox2* and *nanog* [34]. An increased expression of the stemness markers *OCT4*, *SOX2* and *NANOG* increased sarco-spheres and colonies formation in soft agar [35].

On the other hand, the decrease in lactate production in MCF-7 cells treated with BM-MSCs-Exo could be due to the reduction of ROS in these cells. Our results demonstrated that BM-MSCs-Exo can reduce ROS production in these cells. Moreover, studies have indicated that exosomes released by cells are enriched with enzymes such as G6PD [36]. Therefore, exosomes could transfer this enzyme to other cells. The generation of NADPH by G6PD supports

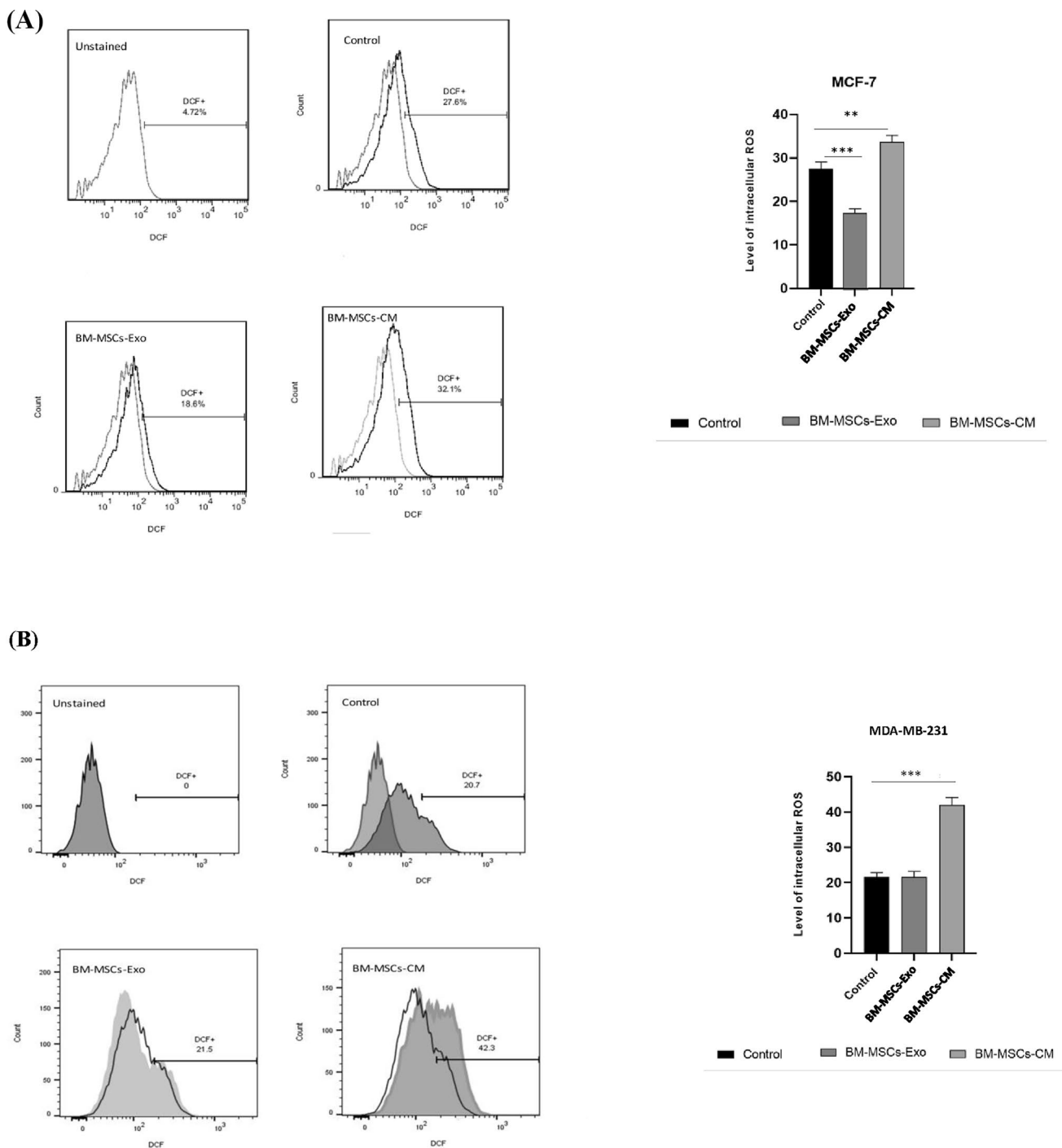


**Fig. 7** Impact of BM-MSCs-Exo and BM-MSCs-CM on ROS generation in breast tumor cells. Panel **A** displays the ROS generation in MCF-7 cells after 24 h of treatment with BM-MSCs-Exo and BM-MSCs-CM, while panel **B** shows the ROS generation in MDA-MB-231 cells. The results are presented as the mean  $\pm$  SD of three independent experiments (\*\* $p < 0.01$  and \*\*\* $p < 0.001$ )

antioxidant systems, thus reducing ROS [33]. G6PD activity was measured to analyze the PPP status of the treatment groups. The results indicated that treatment with BM-MSCs-Exo and BM-MSCs-CM significantly increased G6PD activity compared to the control groups in both cell lines. CSCs,

unlike differentiated cancer cells that show enhanced glycolysis, have distinct metabolic characteristics, including enhanced PPP activity. CSCs play a role in tumor initiation, drug resistance, recurrence, and metastasis, all of which are associated with enhanced PPP activity. For instance,

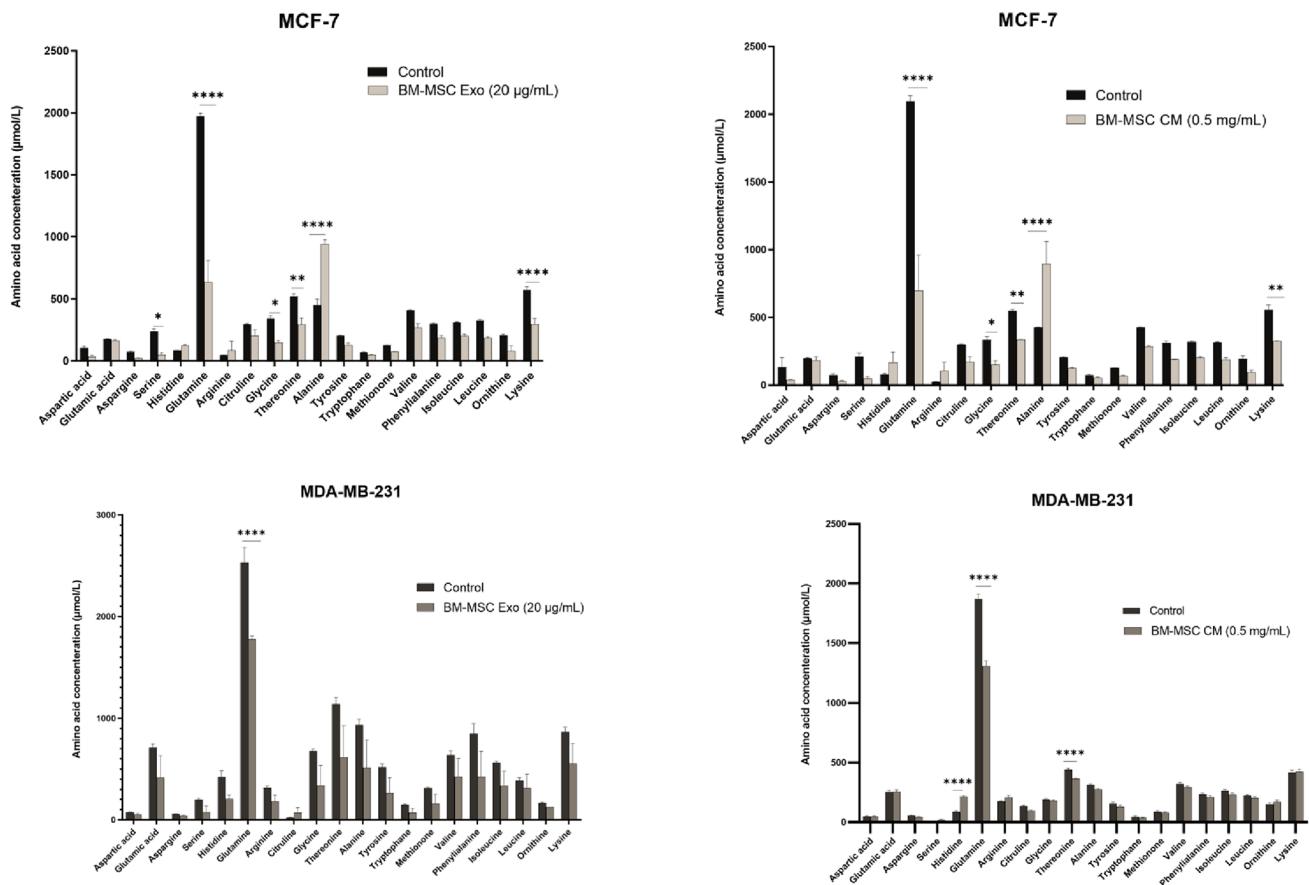


**Fig. 8** The levels of amino acids in MCF-7 and MDA-MB-231 cells were assessed following a 24-h treatment with BM-MSCs-Exo and BM-MSCs-CM. A two-way ANOVA was employed to identify any significant variations in amino acid uptake between the control group

and the treatment groups. The results represent the mean  $\pm$  standard deviation of three independent experiments (\* $p < 0.05$ ; \*\* $p < 0.01$ ; \*\*\* $p < 0.001$ ; \*\*\*\* $p < 0.0001$ )

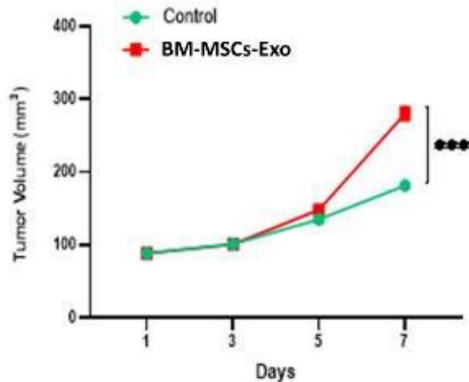
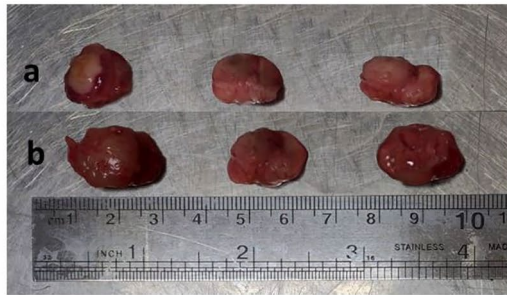
enhanced PPP in tumor cells has been linked to increased drug resistance [22].

Tumor cells, upon encountering ROS, initially activate the glycolysis pathway. Subsequently, with an increase in ROS levels and exposure time, there is a shift in metabolic balance from glycolysis to the PPP [22]. Therefore, the elevation in G6PD activity observed after treatment with conditioned medium from BM-MSCs-CM may be attributed to the heightened presence of ROS within the cells. Similarly, the increase in G6PD activity following treatment with BM-MSCs-Exo could be attributed to the transfer of G6PD via exosomes to target cells.

In this study, we evaluated the levels of 20 amino acids in the conditioned media during treatment with BM-MSCs-Exo and BM-MSCs-CM in MCF-7 and MDA-MB-231 cell lines. The results of the HPLC analysis revealed that the concentration of alanine in the conditioned media of the treatment group was significantly higher than that of the control group in MCF-7 cells. Furthermore, in MDA-MB-231 cells, the concentration of histidine showed a significant increase

compared to the control group. The biosynthesis of histidine is intricately linked to nucleotide metabolism, specifically phosphoribosyl pyrophosphate (PRPP), which is derived from ribose-5-phosphate supplied by PPP. The biosynthesis of histidine branches off from the pentose phosphate metabolism [32, 33]. Additionally, the concentration of 19 amino acids decreased in the conditioned media of MCF-7 cells treated with BM-MSCs-Exo and BM-MSCs-CM, indicating an augmentation in the uptake of these amino acids. Previous studies have suggested that amino acid uptake is enhanced in the cancer stem cell population [18, 30–39]. Clinical trials showed that limiting amino acid intake may improve cancer prognoses [40]. Medications that target amino acid transporters and their associated enzymes have moved from preclinical studies into clinical trials, and some have shown to be effective [41]. Glutamine transporters, which are often highly expressed and linked to a poor prognosis, are essential for the survival of cancer cells, as they require external glutamine [42, 43]. This distinction between cancer cells and normal cells presents a target for cancer treatment. In a

(A)



(B)

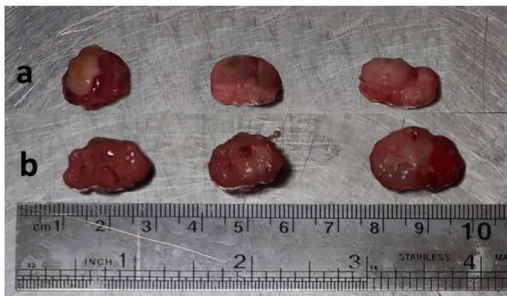
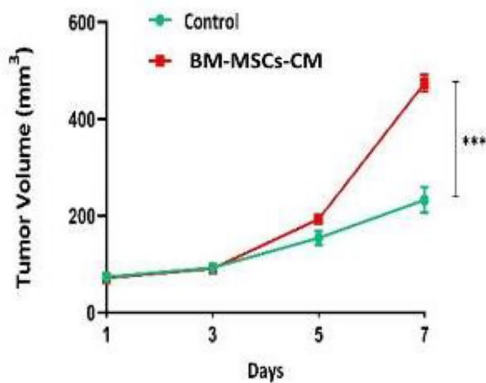


**Fig. 9** The tumor size and volume (mm<sup>3</sup>) in mice challenged with 4T1 cells were examined. The tumor size and volume of the (a) untreated group and (b) the group treated with **A** BM-MSCs-Exo and **B** BM-MSCs-CM after 7 days. Each value represents the mean  $\pm$  standard deviation (n = 6 mice per group) (\*\*\*)  $p < 0.001$

clinical setting, Tamoxifen and Raloxifene work by blocking glutamine absorption through inhibiting ASCT2 expression in breast cancer, thus reducing tumor growth [44].

## Conclusions

In conclusion, our findings demonstrate that the treatment of cancer cells with BM-MSCs-Exo and BM-MSCs-CM can induce metabolic alterations in these cells. Furthermore, the metabolic changes observed in cancer cells under these treatments can promote the acquisition of stem cell characteristics. Both treatments had similar effects on increasing the population of CSCs by affecting different metabolic pathways. The results of this research can improve the identification, targeting and development of new therapeutic methods against CSCs.

**Acknowledgements** We would like to particularly thank Maryam Ghanbari Movahed, Parisa Mohammadi, Alireza Farokhi, and Zohreh Hosseinkhani for their treasured discussions in preparing the manuscript.

**Author contributions** Zahra Ghanbari Movahed: writing—original draft-Lead, Kamran Mansouri: project administration-equal, Ali Hamrahi Mohsen: methodology-equal, Maryam M. Matin: writing—review & editing-equal.

**Funding** This study was supported by a Grant (No. 42771) from Ferdowsi University of Mashhad.

**Data availability** The data that support the findings of this study are available from the corresponding author and author initial, upon reasonable request.

## Declarations

**Competing interests** The authors declare no competing interests.

**Ethical approval** Animal care and handling procedures were conducted in accordance with the regulations of Research Ethics Committee at Kermanshah University of Medical Sciences (IR.KUMS.REC.1396.579).

## References

1. Friedenstein AJ, Chailakhjan RK, Lalykina K. The development of fibroblast colonies in monolayer cultures of guinea-pig bone marrow and spleen cells. *Cell Prolif.* 1970;3(4):393–403.
2. Shi Y, Du L, Lin L, Wang Y. Tumour-associated mesenchymal stem/stromal cells: emerging therapeutic targets. *Nat Rev Drug Discov.* 2017;16(1):35–52.
3. Zhu W, et al. Mesenchymal stem cells derived from bone marrow favor tumor cell growth *in vivo*. *Exp Mol Pathol.* 2006;80(3):267–74.
4. Lee PH, et al. Autologous mesenchymal stem cell therapy delays the progression of neurological deficits in patients with multiple system atrophy. *Clin Pharmacol Ther.* 2008;83(5):723–30.

5. Wakitani S, et al. Safety of autologous bone marrow-derived mesenchymal stem cell transplantation for cartilage repair in 41 patients with 45 joints followed for up to 11 years and 5 months. *J Tissue Eng Regen Med.* 2011;5(2):146–50.
6. Wang L, et al. Human umbilical cord mesenchymal stem cell therapy for patients with active rheumatoid arthritis: safety and efficacy. *Stem Cells Dev.* 2013;22(24):3192–202.
7. Perico L, et al. Human mesenchymal stromal cells transplanted into mice stimulate renal tubular cells and enhance mitochondrial function. *Nat Commun.* 2017;8(1):1–17.
8. Zhu W, et al. Mesenchymal stem cell-secreted soluble signaling molecules potentiate tumor growth. *Cell Cycle.* 2011;10(18):3198–207.
9. Zhu W, et al. Exosomes derived from human bone marrow mesenchymal stem cells promote tumor growth *in vivo*. *Cancer Lett.* 2012;315(1):28–37.
10. Ullah M, Akbar A, Ng NN, Concepcion W, Thakor AS. Mesenchymal stem cells confer chemoresistance in breast cancer via a CD9 dependent mechanism. *Oncotarget.* 2019;5(10):3435.
11. Zhang T, Lee YW, Rui YF, Cheng TY, Jiang XH, Li G. Bone marrow-derived mesenchymal stem cells promote growth and angiogenesis of breast and prostate tumors. *Stem Cell Res Ther.* 2013;4:1–5.
12. De Boeck A, et al. Bone marrow-derived mesenchymal stem cells promote colorectal cancer progression through paracrine neuregulin 1/HER3 signalling. *Gut.* 2013;62(4):550–60.
13. Bliss SA, Sinha G, Sandiford OA, Williams LM, Engelberth DJ, Guiro K, Isenalumhe LL, Greco SJ, Ayer S, Bryan M, Kumar R. Mesenchymal stem cell-derived exosomes stimulate cycling quiescence and early breast cancer dormancy in bone marrow. *Cancer Res.* 2016;1(76):5832–44.
14. Nawaz M, et al. Extracellular vesicles: evolving factors in stem cell biology. *Stem Cells Int.* 2016. <https://doi.org/10.1155/2016/1073140>.
15. Gurung S, Perocheau D, Touramanidou L, Baruteau J. The exosome journey: from biogenesis to uptake and intracellular signalling. *Cell Commun Signal.* 2021;19(1):1–9.
16. Fatima F, Nawaz M. Vesiculated long non-coding RNAs: offshore packages deciphering trans-regulation between cells, cancer progression and resistance to therapies. *Non-coding RNA.* 2017;3(1):10.
17. Nawaz M, et al. The emerging role of extracellular vesicles as biomarkers for urogenital cancers. *Nat Rev Urol.* 2014;11(12):688–701.
18. Tan M, et al. Thrombin stimulated platelet-derived exosomes inhibit platelet-derived growth factor receptor-beta expression in vascular smooth muscle cells. *Cell Physiol Biochem.* 2016;38(6):2348–65.
19. Camussi G, et al. Exosomes/microvesicles as a mechanism of cell-to-cell communication. *Kidney Int.* 2010;78(9):838–48.
20. Yang E, et al. Exosome-mediated metabolic reprogramming: the emerging role in tumor microenvironment remodeling and its influence on cancer progression. *Signal Transduct Target Ther.* 2020;5(1):1–13.
21. Wang X, Yu Z, Zhou X. Metabolic reprogramming in hematological malignancies: advances and clinical perspectives. *Cancer Res.* 2022;82(17):2955–63.
22. Movahed ZG, Rastegari-Pouyani M, Hossein Mohammadi M, Mansouri K. Cancer cells change their glucose metabolism to overcome increased ROS: one step from cancer cell to cancer stem cell? *Biomed Pharmacother.* 2019;1(12):108690.
23. Ho WY, Yeap SK, Ho CL, Rahim RA, Alitheen NB. Development of multicellular tumor spheroid (MCTS) culture from breast cancer cell and a high throughput screening method using the MTT assay. *PLoS ONE.* 2012;7: e44640.
24. Mosmann T. Rapid colorimetric assay for cellular growth and survival: application to proliferation and cytotoxicity assays. *J Immunol Methods.* 1983;65:55–63.
25. Shokoohinia Y, Rashidi M, Hosseinzadeh L, Jelodarian Z. Quercetin-3-O- $\beta$ -d-glucopyranoside, a dietary flavonoid, protects PC12 cells from H<sub>2</sub>O<sub>2</sub>-induced cytotoxicity through inhibition of reactive oxygen species. *Food Chem.* 2015;167:162–7.
26. Li N, Hua J. Interactions between mesenchymal stem cells and the immune system. *Cell Mol Life Sci.* 2017;74:2345–60.
27. Wexler SA, Donaldson C, Denning-Kendall P, Rice C, Bradley B, Hows JM. Adult bone marrow is a rich source of human mesenchymal ‘stem’ cells but umbilical cord and mobilized adult blood are not. *Br J Haematol.* 2003;121(2):368–74.
28. Dazzi F, Ramasamy R, Glennie S, Jones SP, Roberts I. The role of mesenchymal stem cells in haemopoiesis. *Blood Rev.* 2006;20(3):161–71.
29. Jing Y, Liang W, Zhang L, Tang J, Huang Z. The role of mesenchymal stem cells in the induction of cancer-stem cell phenotype. *Front Oncol.* 2022;12: 817971.
30. Tan M, Yan HB, Li JN, Li WK, Fu YY, Chen W, Zhou Z. Thrombin stimulated platelet-derived exosomes inhibit platelet-derived growth factor receptor-beta expression in vascular smooth muscle cells. *Cell Physiol Biochem.* 2016;38(6):2348–65.
31. Camussi G, Deregibus MC, Bruno S, Cantaluppi V, Biancone L. Exosomes/microvesicles as a mechanism of cell-to-cell communication. *Kidney Int.* 2010;78(9):838–48.
32. Hass R. Role of MSC in the tumor microenvironment. *Cancers.* 2020;12(8):2107.
33. Farhadi P, Yarani R, Kiani S, Mansouri K. Perfluorocarbon as an adjuvant for tumor anti-angiogenic therapy: relevance to hypoxia and HIF-1. *Med Hypotheses.* 2021;146: 110357.
34. Kim MC, Cui FJ, Kim Y. Hydrogen peroxide promotes epithelial to mesenchymal transition and stemness in human malignant mesothelioma cells. *Asian Pac J Cancer Prev.* 2013;14(6):3625–30.
35. La Noce M, Paino F, Mele L, Papaccio G, Regad T, Lombardi A, Papaccio F, Desiderio V, Tirino V. HDAC2 depletion promotes osteosarcoma’s stemness both *in vitro* and *in vivo*: a study on a putative new target for CSCs directed therapy. *J Exp Clin Cancer Res.* 2018;37:1–5.
36. Wang W, Zhu N, Yan T, Shi YN, Chen J, Zhang CJ, Xie XJ, Liao DF, Qin L. The crosstalk: exosomes and lipid metabolism. *Cell Commun Signal.* 2020;18(1):1–2.
37. Hecker PA, Lionetti V, Ribeiro RF Jr, Rastogi S, Brown BH, O’Connell KA, Cox JW, Shekar KC, Gamble DM, Sabbah HN, Leopold JA. Glucose 6-phosphate dehydrogenase deficiency increases redox stress and moderately accelerates the development of heart failure. *Circ Heart Fail.* 2013;6(1):118–26.
38. Ohta D, Fujimori K, Mizutani M, Nakayama Y, Kunpaisal-Hashimoto R, Munzer S, Kozaki A. Molecular cloning and characterization of ATP-phosphoribosyl transferase from *Arabidopsis*, a key enzyme in the histidine biosynthetic pathway. *Plant Physiol.* 2000;122:907–14.
39. Stepansky A, Leustek T. Histidine biosynthesis in plants. *Amino Acids.* 2006;30:127–42.
40. Fung MK, Chan GC. Drug-induced amino acid deprivation as strategy for cancer therapy. *J Hematol Oncol.* 2017;10:1–8.
41. Bhutia YD, Babu E, Ramachandran S, Ganapathy V. Amino acid transporters in cancer and their relevance to “glutamine addiction”: novel targets for the design of a new class of anticancer drugs. *Cancer Res.* 2015;75(9):1782–8.
42. Schulte ML, Fu A, Zhao P, Li J, Geng L, Smith ST, Kondo J, Coffey RJ, Johnson MO, Rathmell JC, Sharick JT. Pharmacological blockade of ASCT2-dependent glutamine transport leads to antitumor efficacy in preclinical models. *Nat Med.* 2018;24(2):194–202.
43. Cha YJ, Kim ES, Koo JS. Amino acid transporters and glutamine metabolism in breast cancer. *Int J Mol Sci.* 2018;19(3):907.

44. Peng JB, Zhuang L, Berger UV, Adam RM, Williams BJ, Brown EM, Hediger MA, Freeman MR. CaT1 expression correlates with tumor grade in prostate cancer. *Biochem Biophys Res Commun.* 2001;282(3):729–34.

**Publisher's Note** Springer Nature remains neutral with regard to jurisdictional claims in published maps and institutional affiliations.

Springer Nature or its licensor (e.g. a society or other partner) holds exclusive rights to this article under a publishing agreement with the author(s) or other rightsholder(s); author self-archiving of the accepted manuscript version of this article is solely governed by the terms of such publishing agreement and applicable law.